Contribution from the School of Chemical Sciences,
University of Illinois, Urbana, Illinois 61801

# Dynamics of Spin-State Interconversion and Cooperativity for Ferric Spin-Crossover Complexes in the Solid State. 4.[1] Pyruvic Acid Thiosemicarbazone Complex

MARK D. TIMKEN, SCOTT R. WILSON, and DAVID N. HENDRICKSON*

*Received January 15, 1985*

The preparation and characterization of the new discontinuous ferric spin-crossover complex [Fe(Hthpu)(thpu)], the hydrated low-spin form of the complex [Fe(Hthpu)(thpu)]·$H_2O$, and the analogous hydrated $Cr^{III}$ complex are reported. In these complexes, $Hthpu^-$ and $thpu^{2-}$ are deprotonated forms of pyruvic acid thiosemicarbazone; each is an ONS tridentate ligand. The X-ray structure of [Cr(Hthpu)(thpu)]·$H_2O$ has been determined by using direct methods, in conjunction with data measured on a four-circle diffractometer, to give discrepancy factors of $R_F = 0.030$ and $R_{wF} = 0.034$ for 1766 observed ($|F|^2 > 2.58\sigma|F|^2$) reflections. The compound crystallizes in the monoclinic space group $P2_1/n$ with four formula weights in a cell having the dimensions $a = 11.174$ (2) Å, $b = 10.674$ (2) Å, $c = 13.194$ (3) Å, and $\beta = 103.14$ (2)°. The observed and calculated densities are 1.66 and 1.687 g cm$^{-3}$, respectively. The molecular structure of [Cr(Hthpu)(thpu)] in this hydrate is found to be that of an appreciably distorted octahedral complex. The chemical inequivalence of the two ligands was clearly established, for the "extra" hydrogen atom on the thione ligand $Hthpu^-$ was found to be bound to the noncoordinated nitrogen atom. The thiol ligand $thpu^{2-}$ binds more tightly to the $Cr^{III}$ ion than does the thione ligand, as evidenced by metal–ligand distances that are shorter for the thiol form than for the thione form. There is a three-dimensional network of hydrogen bonds in [Cr(Hthpu)(thpu)]·$H_2O$. The discontinuous spin-crossover transformation shows a thermal hysteresis, where with sample cooling the transition temperature is 225 K and with sample heating it is 235 K. Variable-temperature magnetic susceptibility, EPR, and $^{57}$Fe Mössbauer results indicate the presence of a first-order phase transition. It is very likely that the cooperative (i.e., first-order) nature of this transition is due to the extended coupling of ferric complexes through *inter*molecular hydrogen-bonding interactions.

## Introduction

Thermally discontinuous spin-crossover transformations are those for which the high-spin to low-spin transition occurs sharply over a temperature interval of only a few degrees. These discontinuous transformations, which cannot be understood in terms of a simple Boltzmann equilibrium between noninteracting low- and high-spin electronic states, have been reported[2] for a variety of spin-crossover compounds. Observations of thermal hysteresis,[2] as well as a very few heat capacity investigations,[3-5] have identified most of these transformations as thermodynamic first-order phase transitions.[6] Variable-temperature X-ray powder diffraction techniques have also recently revealed that discontinuous lattice modifications (and concomitant unit cell volume changes) accompany these spin-crossover transformations.[7-9] These observations are in keeping with the first-order character of such transitions. Although relatively little is understood about the *microscopic* mechanisms of these transitions, cooperative (i.e., *inter*molecular) interactions are surely of importance.

Of the variety of six-coordinate *ferric* spin-crossover compounds discovered so far, relatively few exhibit transformations of the discontinuous type. Haddad et al.[10-12] have prepared [Fe(3-OMeSalEen)$_2$]$PF_6$, where 3-OMeSalEen is the monoanion of the Schiff-base condensate of 3-methoxysalicylaldehyde and *N*-ethylethylenediamine. This compound undergoes a discontinuous transformation at 161 K. *As a class*, only the ferric thiosemicarbazones show a number of discontinuous spin-crossover examples.[13-17] The thiosemicarbazones are also unique among ferric spin-crossover compounds in that they exhibit distinct and narrow $^{57}$Fe Mössbauer absorptions for the high- and low-spin electronic states.[14,18,19] Two types of ferric thiosemicarbazone compounds possess spin-crossover properties, the pyruvic acid thiosemicarbazones (I) and the salicylaldehyde thiosemicarbazones (II).

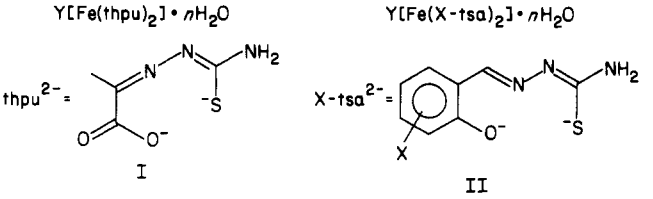


I II

For these compounds the spin-state properties are quite sensitive to changes in the counterion Y (typically an alkali-metal cation or a protonated nitrogenous base), the number of hydrates, and the nature of the salicylaldehyde substituent X. The spin-crossover properties of these compounds have been characterized primarily through variable-temperature magnetic susceptibility and $^{57}$Fe Mössbauer investigations. Recently, variable-temperature single-crystal X-ray structures have also been reported[20-23] for several of the ferric salicylaldehyde thiosemicarbazones.

In the continuation of our recent efforts[10-12] to understand the solid-state features that control spin-crossover properties, we were motivated to investigate the thermally discontinuous spin-state transitions in these ferric thiosemicarbazones. In the course of

(1) Part 3: Timken, M. D.; Hendrickson, D. N.; Sinn, E. *Inorg. Chem.*, in press.
(2) Gütlich, P. *Struct. Bonding (Berlin)* **1981**, *44*, 83.
(3) Sorai, M.; Seki, S. *J. Phys. Soc. Jpn.* **1972**, *33*, 575.
(4) Sorai, M.; Seki, S. *J. Phys. Chem. Solids* **1974**, *35*, 555.
(5) Shipilov, V. I.; Zelentsov, V. V.; Zhadanov, V. M.; Turdakin, V. A. *JETP Lett. (Engl. Transl.)* **1974**, *19*, 294.
(6) Kittel, C.; Kroemer, H. "Thermal Physics"; W. H. Freeman Co.: San Francisco, CA, 1980; Chapter 10.
(7) Irler, W.; Ritter, G.; König, E.; Goodwin, H. A.; Nelson, S. M. *Solid State Commun.* **1979**, *29*, 39.
(8) König, R.; Ritter, G.; Irler, W.; Goodwin, H. A. *J. Am. Chem. Soc.* **1980**, *102*, 4681.
(9) (a) König, E.; Ritter, G.; Kulshreshtha, S. K.; Waigel, J.; Goodwin, H. A. *Inorg. Chem.* **1984**, *23*, 1896. (b) König, E.; Ritter, G.; Kulshreshtha, S. K. *Chem. Rev.* **1985**, *85*, 219.
(10) Haddad, M. S.; Lynch, M. W.; Federer, W. D.; Hendrickson, D. N. *J. Am. Chem. Soc.* **1980**, *102*, 1468.
(11) Haddad, M. S.; Lynch, M. W.; Federer, W. D.; Hendrickson, D. N. *Inorg. Chem.* **1981**, *20*, 123.
(12) Haddad, M. S.; Federer, W. D.; Lynch, M. W.; Hendrickson, D. N. *Inorg. Chem.* **1981**, *20*, 131.
(13) Ivanov, E. V.; Zelentsov, V. V.; Gerbeleu, N. V.; Ablov, A. V. *Dokl. Chem. (Engl. Transl.)* **1970**, *191*, 249.
(14) Zelentsov, V. V.; Ablov, A. V.; Turta, K. I.; Stukan, R. A.; Gerbeleu, N. V.; Ivanov, E. V.; Bogdanov, A. P.; Barba, N. A.; Bodyu, V. G. *Russ. J. Inorg. Chem. (Engl. Transl.)* **1972**, *17*, 1000.
(15) Zelentsov, V. V.; Bogdanova, L. G.; Ablov, A. V.; Gerbeleu, N. V.; Dyatlova, Ch. V. *Dokl. Chem. (Engl. Transl.)* **1972**, *207*, 864.
(16) Zelentsov, V. V.; Larin, G. M.; Ivanov, E. V.; Gerbeleu, N. V.; Ablov, A. V. *Theor. Exp. Chem. (Engl. Transl.)* **1971**, *7*, 648.
(17) Ablov, A. V.; Zelentsov, V. V.; Shipilov, V. I.; Gerbeleu, N. V.; Dyatlova, Ch. V. *Dokl. Phys. Chem. (Engl. Transl.)* **1975**, *222*, 567.
(18) Turta, K. I.; Ablov, A. V.; Gerbeleu, N. V.; Dyatlova, Ch. V.; Stukan, R. A. *Russ. J. Inorg. Chem. (Engl. Transl.)* **1976**, *21*, 266.
(19) Ablov, A. V.; Goldanskii, V. I.; Turta, K. I.; Stukan, R. A.; Zelentsov, V. V.; Ivanov, E. V.; Gerbeleu, N. V. *Dokl. Phys. Chem. (Engl. Transl.)* **1971**, *196*, 134.
(20) Ryabova, N. A.; Ponomarev, V. I.; Atovmyan, L. O.; Zelentsov, V. V.; Shipilov, V. I. *Sov. J. Coord. Chem. (Engl. Transl.)* **1978**, *4*, 95.
(21) Ryabova, N. A.; Ponomarev, V. I.; Zelentsov, V. V.; Atovmyan, L. O. *Sov. Phys.—Crystallogr. (Engl. Transl.)* **1981**, *26*, 53.
(22) Ryabova, N. A.; Ponomarev, V. I.; Zelentsov, V. V.; Atovmyan, L. O. *Sov. Phys.—Crystallogr. (Engl. Transl.)* **1982**, *27*, 46.
(23) Ryabova, N. A.; Ponomarev, V. I.; Zelentsov, V. V.; Atovmyan, L. O. *Sov. Phys.—Crystallogr. (Engl. Transl.)* **1982**, *27*, 171.

0020-1669/85/1324-3450$01.50/0 

this work we synthesized the two new compounds [Fe(Hthpu)(thpu)]·$n$$H_2O$ where $n$ = 0, 1. Variable-temperature magnetic and spectroscopic characterizations of the spin-crossover transition in the nonhydrated compound are reported in this paper. The molecular and solid-state factors that lead to the discontinuous nature of the spin-state transition in this compound are discussed.

In addition, the unusual feature of the inequivalent ligands $Hthpu^-$ and $thpu^{2-}$ motivated us to characterize structurally the previously reported[24] compound [Cr(Hthpu)(thpu)]·$H_2O$. Although metal thiosemicarbazones with similarly inequivalent ligands have been reported,[16,19,25-27] the single-crystal X-ray results described here represent the first structural characterization of such a complex. Consequently, we are able to describe the systematic structural differences between the $Hthpu^-$ (thione) and $thpu^{2-}$ (thiol) ligand forms as they are bound to the same metal center.

## Experimental Section

**Compound Preparation.** Commercially available starting materials were used without further purification. Elemental analyses were performed in the Microanalytical Laboratory of the School of Chemical Sciences, University of Illinois.

**Thiosemicarbazide Hydrochloride.** A typical preparation consisted of adding 4 mL of concentrated HCl to a slurry of 4.4 g of powdered thiosemicarbazide in 80 mL of ethanol. The slurry was stirred overnight, and the white powdery product was isolated by filtration and washed with ethanol.

**$H_2$thpu·$^1/_2H_2O$.** Pyruvic acid thiosemicarbazone was prepared following the method of Freund and Schander.[28] A solution of 0.88 g of pyruvic acid in 10 mL of $H_2O$ was added dropwise with stirring to 1.28 g of thiosemicarbazide hydrochloride in 10 mL of $H_2O$. The white, microcrystalline product was isolated by filtration, washed with $H_2O$, and dried in vacuo. Anal. Calcd for $C_4N_3O_{2.5}SH_8$: C, 28.23; H, 4.74; N, 24.70. Found: C, 28.13; H, 4.69; N, 24.58. For the following reactions, we found that it was best to use freshly prepared $H_2$thpu·$^1/_2H_2O$.

**[Fe(Hthpu)(thpu)].** All of the steps were carried out at room temperature. A slurry of $H_2$thpu·$^1/_2H_2O$ was prepared by stirring 0.29 g of the microcrystalline solid in 40 mL of $H_2O$ containing 5.2 g of KCl. To this slurry was added dropwise with stirring a solution of 2.85 g of $Fe(NO_3)_3$·$9H_2O$ in 50 mL of $H_2O$. As the addition proceeded, the slurry gradually changed color from white to green to brown, and dark brown microcrystals formed. After the addition of the last of the ferric solution, the reaction mixture was stirred for an additional 10 min. The product was isolated by filtration, washed with large quantities of $H_2O$, and allowed to air-dry overnight to give 2.2 g (83% yield) of dark brown microcrystals. Anal. Calcd for $FeO_4S_2N_6C_8H_9$: C, 25.61; H, 2.96; N, 22.40; Fe, 14.88. Found: C, 25.34; H, 3.05; N, 21.91; Fe, 14.73.

Approximately 0.5 g of the microcrystalline product was divided into four portions, and each portion was ground in a ceramic mortar and pestle for 2 min to give a total of 0.49 g of green powder. Anal. Calcd for $FeO_4S_2N_6C_8H_9$: C, 25.61; H, 2.96; N, 22.40; Fe, 14.88. Found: C, 25.69; H, 2.75; N, 22.36; Fe, 14.24.

**[Fe(Hthpu)(thpu)]·$H_2O$.** As above, all of the steps were carried out at room temperature. To 1.0 g of $H_2$thpu·$^1/_2H_2O$ in 300 mL of $H_2O$ was added 0.25 g of $NaHCO_3$ in 5 mL of $H_2O$. The resulting solution was stirred for 2–3 min. A solution of 1.2 g of $Fe(NO_3)_3$·$9H_2O$ in 50 mL of $H_2O$ was added dropwise with stirring to the thiosemicarbazone solution. The dark brown, microcrystalline product was isolated by filtration, washed with $H_2O$, and air-dried to give a yield of 0.89 g (83%). Anal. Calcd for $FeO_5S_2N_6C_8H_{11}$: C, 24.43; H, 3.34; N, 21.38; Fe, 14.20. Found: C, 24.25; H, 3.21; N, 21.02; Fe, 14.26.

An identical material was obtained by performing the reaction in a total volume of 1 L of $H_2O$ in the absence of $NaHCO_3$.

**[Cr(Hthpu)(thpu)]·$H_2O$.** This compound, prepared previously[24] by Ablov et al., was synthesized by the addition of 0.63 g of $Cr(NO_3)_3$·$9H_2O$ in 20 mL of $H_2O$ dropwise to a nearly boiling slurry of 0.5 g of $H_2$thpu·$^1/_2H_2O$ in 20 mL of $H_2O$. Upon boiling, the original deep blue solution turned purple, and dark purple microcrystals precipitated. the reaction mixture was cooled slowly to room temperature, and the product was isolated as above to give 0.25 g (41%). Anal. Calcd for $CrO_5S_2N_6C_8H_{11}$: C, 24.67; H, 3.37; N, 21.59. Found: C, 24.71; H, 3.41; N, 21.63.

Crystals suitable for single-crystal X-ray diffraction studies were isolated by preparing a saturated solution of the complex in boiling $H_2O$. Subsequent slow cooling of this solution in a preheated Dewar afforded small, but suitable, crystals.

Attempts to prepare the nonhydrated form of the chromium complex by carrying out the above reaction at room temperature led to a dark pink powder. The product was characterized to be the hydrated complex by powder X-ray diffraction and elemental analysis.

**Table I.** Experimental and Crystal Data for X-ray Structure of [Cr(Hthpu)(thpu)]·$H_2O$

| Crystal Parameters | |
|---|---|
| cryst syst: monoclinic | space group: $P2_1/n$ |
| $a$ = 11.174 (2) Å | $\alpha$ = 90° |
| $b$ = 10.674 (2) Å | $\beta$ = 103.14 (2)° |
| $c$ = 13.194 (3) Å | $\gamma$ = 90° |
| $V$ = 1532.5 (6) Å$^3$ | $Z$ = 4 |
| fw = 389.35 | $\mu$ = 10.19 cm$^{-1}$ |
| $\rho$(calcd) = 1.687 g cm$^{-3}$ | $\rho$(expt) = 1.66 g cm$^{-3}$ |

| Data Measurement |
|---|
| diffractometer: four-circle Syntex $P2_1$ |
| radiation: graphite monochromatized Mo K$\alpha$ ($\lambda$ = 0.71069 Å) |
| $2\theta$ limits: 3.0° < $2\theta$ < 50.0° |
| scan range: −0.8 to +1.0° |
| data measd: 2722 ($\pm h,k,l$) |
| data used: $\lvert F\rvert^2 > 2.58\sigma\lvert F\rvert^2$, 1766 reflcns |
| transmission factor limits: 0.717–0.911 |
| internal consistency: $R_i$ = 0.012 |
| $R_F$[a] = 0.030 |
| $R_{wF}$[a] = 0.034 |

[a] $R_F = \sum\lvert F_o - \lvert F_c\rvert\rvert/\sum F_o$; $R_{wF} = [\sum w(F_o - \lvert F_c\rvert)^2/\sum wF_o^2]^{1/2}$.

## Physical Measurements

Variable-temperature magnetic susceptibility data were obtained on two instruments. For the mortar and pestle ground sample (vide supra), a PAR Model 150A vibrating-sample magnetometer, operated at 13.5 kG, was used. The magnetometer was calibrated with $CuSO_4$·$5H_2O$, and a calibrated GaAs diode was used for sample temperature determination and control. Other samples were examined with the use of a Series 800 VTS-50 SQUID susceptometer (SHE Corp.). A magnetic field of 10 kG was used. For all data, diamagnetic corrections, estimated from Pascal's constants, were used in the calculation of molar paramagnetic susceptibilities.

Electron paramagnetic resonance data (X-band) were collected with the use of a Varian E-9 spectrometer. Variable temperatures (300–130 K) were obtained with the use of a gas-flow cavity insert in conjunction with a Varian V-4540 temperature controller. Absolute temperature accuracy is estimated to be no better than ±5 K, although the relative precision is much better (±0.5 K). Signal intensities of derivative features were estimated from peak-to-peak heights.[29] Spectra at Q-band frequencies were collected on a Varian E-15 spectrometer. Low temperatures were achieved by inserting the entire cavity into a gas-flow cryostat.

Mössbauer ($^{57}$Fe) spectra were run as previously described.[30,31] We estimate the absolute temperature precision to be ±3 K; the relative precision is ±0.5 K. Magnetically perturbed spectra were obtained with the use of a superconducting magnet situated with the applied field parallel to the direction of $\gamma$-ray propagation. The operational details of collecting applied-field spectra are described elsewhere.[30] The zero-field Mössbauer absorptions were least-squares fit to Lorentzian line shapes with a previously documented[32] computer program. Isomer shift data are reported relative to those of iron foil at 298 K but are not corrected for temperature-dependent second-order Doppler effects. It should be noted that the isomer shifts illustrated in the figures are displaced slightly from the actual values and, as such, accurate isomer shift

(24) Ablov, A. V.; Gerbeleu, N. V. *Russ. J. Inorg. Chem.* (*Engl. Transl.*) **1970**, *15*, 952.
(25) Ablov, A. V.; Gerbeleu, N. V. *Russ. J. Inorg. Chem.* (*Engl. Transl.*) **1964**, *9*, 1260.
(26) Ablov, A. V.; Bologa, O. A. *Russ. J. Inorg. Chem.* (*Engl. Transl.*) **1977**, *22*, 127.
(27) Bologa, O. A.; Belichuk, N. I.; Ablov, A. V. *Russ. J. Inorg. Chem.* (*Engl. Transl.*) **1978**, *23*, 1036.
(28) Freund, M.; Schander, A. *Ber. Dtsch. Chem. Ges.* **1902**, *35*, 2602.
(29) Wertz, J. E.; Bolton, J. R. "Electron Spin Resonance"; McGraw-Hill: New York, 1972; p 34.
(30) Cohn, M. J.; Timken, M. D.; Hendrickson, D. N. *J. Am. Chem. Soc.* **1984**, *106*, 6683.
(31) Federer, W. D.; Hendrickson, D. N. *Inorg. Chem.* **1984**, *23*, 3861.
(32) Chrisman, B. L.; Tumolillo, T. A. *Comput. Phys. Commun.* **1971**, *2*, 322.

**Table II.** Positional Parameters for [Cr(Hthpu)(thpu)]·$H_2O$[a]

| | x/a | y/b | z/c |
|---|---|---|---|
| Cr | 0.57247 (5) | 0.02719 (5) | 0.24685 (4) |
| S1 | 0.69075 (8) | 0.09663 (9) | 0.40863 (7) |
| S2 | 0.73928 (9) | −0.07979 (9) | 0.20016 (7) |
| O1 | 0.4527 (2) | −0.0636 (2) | 0.1406 (2) |
| O2 | 0.3214 (2) | −0.2229 (2) | 0.1190 (2) |
| O3 | 0.4453 (2) | 0.1549 (2) | 0.2522 (2) |
| O4 | 0.3811 (2) | 0.3448 (3) | 0.1952 (2) |
| O5 | 0.4496 (3) | 0.3426 (3) | 0.4262 (3) |
| N1 | 0.7001 (3) | −0.0272 (4) | 0.5821 (2) |
| N2 | 0.5754 (3) | −0.1222 (3) | 0.4424 (2) |
| N3 | 0.5267 (2) | −0.1082 (3) | 0.3372 (2) |
| N4 | 0.8349 (3) | −0.0032 (3) | 0.0453 (3) |
| N5 | 0.6920 (3) | 0.1292 (3) | 0.0835 (2) |
| N6 | 0.6046 (2) | 0.1514 (3) | 0.1393 (2) |
| C1 | 0.6508 (3) | −0.0277 (3) | 0.4798 (2) |
| C2 | 0.4444 (3) | −0.1867 (3) | 0.2890 (3) |
| C3 | 0.4014 (3) | −0.1577 (3) | 0.1745 (3) |
| C4 | 0.3953 (5) | −0.2952 (5) | 0.3367 (4) |
| C5 | 0.7562 (3) | 0.0203 (3) | 0.1025 (3) |
| C6 | 0.5332 (3) | 0.2474 (3) | 0.1220 (3) |
| C7 | 0.4450 (3) | 0.2522 (3) | 0.1945 (3) |
| C8 | 0.5335 (5) | 0.3481 (5) | 0.0453 (4) |
| H1 | 0.694 (3) | −0.083 (3) | 0.612 (3) |
| H2 | 0.760 (4) | 0.031 (4) | 0.608 (3) |
| H3 | 0.452 (4) | −0.355 (4) | 0.355 (3) |
| H4 | 0.328 (4) | −0.327 (5) | 0.294 (4) |
| H5 | 0.363 (5) | −0.0261 (5) | 0.394 (4) |
| H6 | 0.882 (4) | −0.075 (5) | 0.065 (4) |
| H7 | 0.855 (3) | 0.056 (4) | 0.011 (3) |
| H8 | 0.683 (3) | 0.162 (3) | 0.027 (3) |
| H9 | 0.605 (5) | 0.350 (5) | 0.020 (4) |
| H10 | 0.471 (5) | 0.331 (5) | −0.004 (4) |
| H11 | 0.514 (5) | 0.421 (6) | 0.075 (5) |
| H12 | 0.452 (5) | 0.280 (5) | 0.456 (4) |
| H13 | 0.416 (4) | 0.340 (5) | 0.373 (4) |

[a] Estimated standard deviations for last significant figure are given in parentheses.

values are to be found in the tabulated results. Magnetically perturbed Mössbauer spectra were computer simulated with the use of a spin-Hamiltonian ($S = {}^1/_2$) program described in detail elsewhere.[30,33]

Infrared spectra were obtained on pressed KBr pellets with the use of a Perkin-Elmer 599B spectrometer.

X-ray powder diffraction patterns were obtained on a Norelco (Phillips Electronics Co.) powder diffractometer equipped with a copper X-ray tube and a graphite monochromator.

**Crystal Measurements and Data Collection.** A tabular transparent red crystal of [Cr(Hthpu)(thpu)]·$H_2O$ (0.10 × 0.30 × 0.42 mm) was used for data collection at 25 °C. The unit cell parameters, listed in Table I, were obtained by a least-squares fit to the automatically centered settings for 15 reflections. Details of data collection may also be found in Table I. No evidence for crystal decomposition was noted. The data were corrected for Lorentz, polarization, and anomalous dispersion effects. Numerical absorption and empirical extinction corrections were also applied.

**Structure Solution and Refinement.** The structure was solved by using direct methods (MULTAN). Correct positions for 20 of the 21 non-hydrogen atoms were deduced from an $E$ map. Subsequent least-squares difference Fourier calculations revealed positions for all of the remaining atoms. In the final cycle of least-squares analysis, all non-hydrogen atom positions were refined with anisotropic thermal coefficients, all hydrogen atom positions were refined with isotropic thermal parameters, and an isotropic empirical extinction coefficient was refined. The final difference Fourier map was featureless.

The final positional parameters for all atoms can be found in Table II. Listings of the thermal parameters and observed and calculated structure factors are available.[34]

## Results and Discussion

**Molecular and Crystal Structure of [Cr(Hthpu)(thpu)]·$H_2O$.** A perspective view of the neutral chromium(III) complex is illustrated in Figure 1. As indicated by the bond angles listed in Table III, the six-coordinate complex is appreciably distorted from ideal octahedral geometry. In particular, the S2–Cr–O3 and S1–Cr–O1 angles are contracted relative to the idealized angle of 180°. It is likely that these contractions originate in the relatively small "bite size" of each of the tridentate chelates.

A major motivation for this crystallographic study was to characterize the structural differences between the two ligands $Hthpu^-$ and $thpu^{2-}$. Both ligands are obtained by sequentially deprotonating neutral pyruvic acid thiosemicarbazone. The chemical inequivalence of the two ligands is evident from Figure

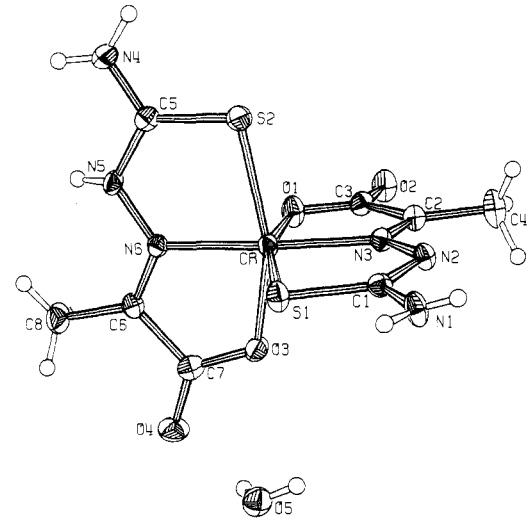


**Figure 1.** Perspective view of [Cr(Hthpu)(thpu)] and hydrate water.

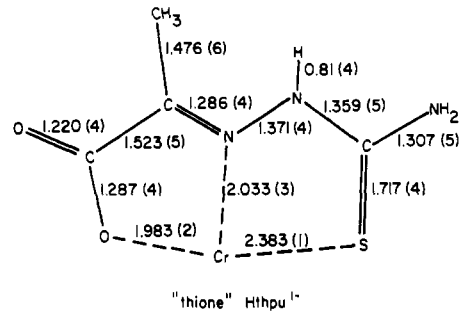


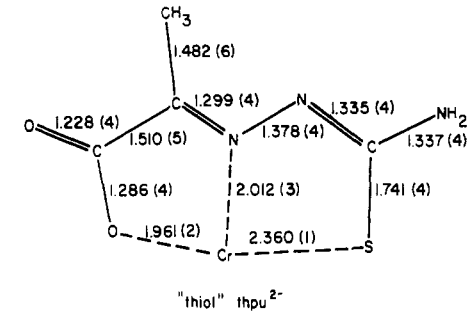


**Figure 2.** Important bond distances (Å) for the Cr–thione and Cr–thiol fragments.

**Table III.** Selected Bond Angles (deg) for [Cr(Hthpu)(thpu)]·$H_2O$

| | | | |
|---|---|---|---|
| S1–Cr–S2 | 94.25 (4) | O1–Cr–N3 | 81.1 (1) |
| S1–Cr–N3 | 81.66 (8) | O3–Cr–N6 | 79.5 (1) |
| S2–Cr–O3 | 161.43 (8) | S1–Cr–O3 | 90.58 (7) |
| O1–Cr–O3 | 89.28 (10) | S2–Cr–O1 | 91.45 (8) |
| O3–Cr–N3 | 101.1 (1) | S2–Cr–N6 | 81.92 (8) |
| S1–Cr–O1 | 162.37 (8) | O1–Cr–N6 | 91.3 (1) |
| S1–Cr–N6 | 105.97 (8) | N3–Cr–N6 | 172.4 (1) |
| S2–Cr–N3 | 97.39 (8) | | |

(33) Münck, E.; Groves, J. L.; Tumolillo, T. A.; Debrunner, P. G. *Comput. Phys. Commun.* **1973**, *5*, 225.
(34) Supplementary material.

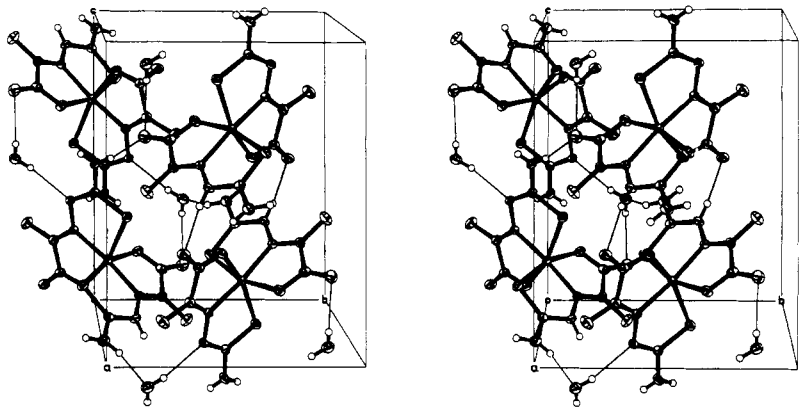

**Figure 3.** Stereoscopic view of the unit cell for $[Cr(Hthpu)(thpu)]\cdot H_2O$. Hydrogen bonds are shown as single solid lines.

**Table IV.** Hydrogen-Bonding Interactions in $[Cr(Hthpu)(thpu)]\cdot H_2O$

| interaction | dist, Å | angle, deg | interaction | dist, Å | angle, deg |
|---|---|---|---|---|---|
| O5–H12···N2[a] | 2.973 (4) | 166 (5) | N1–H2···O4[c] | 2.936 (4) | 167 (4) |
| O5–H13···O4 | 2.969 (4) | 159 (5) | N4–H6···O5[d] | 2.870 (5) | 145 (4) |
| N5–H8···O2[b] | 2.822 (4) | 171 (4) | N4–H7···O5[e] | 2.822 (5) | 161 (3) |

[a] $1-x, -y, 1-z$. [b] $1-x, -y, -z$. [c] $^1/_2+x, ^1/_2-y, ^1/_2+z$. [d] $^3/_2-x, ^{-1}/_2+y, ^1/_2-z$. [e] $^1/_2+x, ^1/_2-y, ^{-1}/_2+z$.

1. The singly deprotonated thione ligand ($Hthpu^-$) possesses a hydrogen atom bound to the N5 nitrogen atom, whereas no such hydrogen atom is found at the N2 position of the doubly deprotonated thiol form of the ligand.

Specific structural differences between the thiol and thione ligands, as well as differences in the manner in which each binds to the chromium center, are illustrated in Figure 2. As expected from electrostatic considerations, the dianionic thiol ligand is bound more tightly to the chromium ion than is the monoanionic thione chelate. It is interesting that the three metal–ligand distances are *uniformly* 0.02 Å shorter for the thiol form than for the thione form. Although the $Hthpu^-$ and $thpu^{2-}$ forms are easily identified by the presence (or lack) of a hydrogen atom at position N5 (or N2), several additional structural features differentiate the two ligand forms. For example, for the thione form the C–S bond is 0.024 Å shorter than the thiol form. Figure 2 also reveals that the thione C5–N5 bond is 0.024 Å larger than the corresponding C1–N2 thiol bond. The C1–N1 and C5–N4 bond distances also differ significantly for the thiol and thione ligands, respectively. There are relatively few crystal structures of metal–thiosemicarbazone complexes with which to compare these observations.[35,36] A preliminary structure report[37] for $Ba[Cr(thpu)_2]_2\cdot 5H_2O$ is not particularly useful due to the poor level of refinement ($R = 0.175$). And although several spin-crossover ferric salicylaldehyde thiosemicarbazones have been structurally characterized,[20-23] details of the analyses suffer due to complications from the spin-crossover transformation. The best comparisons are to be made to the six-coordinate nickel complex[38] bis(isoquinoline-1-carboxaldehyde thiosemicarbazonato)nickel(II) hydrate and to the four-coordinate zinc complex[39] bis(acetone thiosemicarbazone)zinc(II) dichloride. For the nickel complex, both ligands are of the thiol form. The C1–S1 distance is 1.727 Å, the C1–N2 distance is 1.329 Å, and the C1–N1 distance is 1.347 Å. For the zinc complex, the single chelate is of the thione form, and the relevant bond distances are 1.712 Å for C5–S2, 1.392 Å for C5–N5, and 1.313 Å for C5–N4. It is clear that the same systematic differences between the thione and thiol ligands that we pointed out for $[Cr(Hthpu)(thpu)]\cdot H_2O$ are also evident in the comparison of the nickel (thiol) and zinc (thione) structures.

As illustrated in Figure 3, the $[Cr(Hthpu)(thpu)]\cdot H_2O$ lattice is held together by a three-dimensional network of hydrogen bonds. These interactions, listed in Table IV, involve virtually every site that can potentially participate in a hydrogen bond. As we will discuss in more detail (vide infra), it is likely that the hydrogen-bonding interactions strongly influence the nature of the spin-crossover transformation in ferric thiosemicarbazones. The hydrogen-bonding network also holds the chromium centers in close proximity; the three closest Cr–Cr contacts are 6.371 (1), 6.639 (1), and 8.978 (1) Å. The short electron-spin relaxation times that we observe in the electron paramagnetic resonance and $^{57}Fe$ Mössbauer examinations of the analogous ferric pyruvic acid thiosemicarbazones (vide infra) are very likely due to similarly short metal–metal distances.

**Relative Structures of $[Cr(Hthpu)(thpu)]\cdot H_2O$, $[Fe(Hthpu)(thpu)]\cdot H_2O$, and $[Fe(Hthpu)(thpu)]$.** Due to the general insolubility of the two ferric samples and the tendency of each to decompose in solution, we were unable to grow single crystals suitable for X-ray diffraction studies. Consequently, it is difficult to know the precise molecular and solid-state structural features of these materials. Not surprisingly, however, room-temperature X-ray powder diffraction patterns (Figure 4) of the hydrated chromium and hydrated ferric solids indicate that the two materials are isostructural. It is also evident from Figure 4 that the nonhydrated ferric solid is not isostructural to either of the hydrated materials. This latter observation is not surprising in light of the significant role that water molecules play in forming the extensive hydrogen-bonding network found in the chromium structure.

Infrared spectra of the three solids are quite similar. The hydrated ferric and chromium materials show virtually superimposable infrared absorption patterns over the entire frequency range (4000–400 $cm^{-1}$). The IR spectrum of the nonhydrated ferric material is very similar to those of the hydrated materials in the region below 2000 $cm^{-1}$. Above 2000 $cm^{-1}$, the region in which symmetric and asymmetric N–H stretches absorb, the spectra for the hydrated and nonhydrated forms show clear differences. Undoubtedly, the presence or lack of water in the lattice changes the nature of the hydrogen bonding. These differences in hydrogen bonding are manifested in frequency shifts in the N–H stretching region.

From these observations, we infer that the *molecular* structure of the [M(Hthpu)(thpu)] unit in all three solids is essentially identical. On the other hand, the *lattice* structures of the hydrated and nonhydrated materials are certainly different.

**Low-Spin Forms of $[Fe(Hthpu)(thpu)]\cdot H_2O$ and $[Fe(Hthpu)(thpu)]$.** The hydrated ferric material is low-spin, whereas the

(35) Campbell, M. J. M. *Coord. Chem. Rev.* **1975**, *15*, 279.
(36) Padhye, S.; Kauffman, G. *Coord. Chem. Rev.* **1985**, *63*, 127.
(37) Volodina, G. F.; Kiosse, G. A.; Gerbeleu, N. V.; Ablov, A. V. *Dokl. Chem. (Engl. Transl.)* **1971**, *200*, 853.
(38) Mathew, M.; Palenik, G. J. *J. Am. Chem. Soc.* **1969**, *91*, 6310.
(39) Mathew, M.; Palenik, G. J. *Inorg. Chim. Acta* **1971**, *5*, 349.

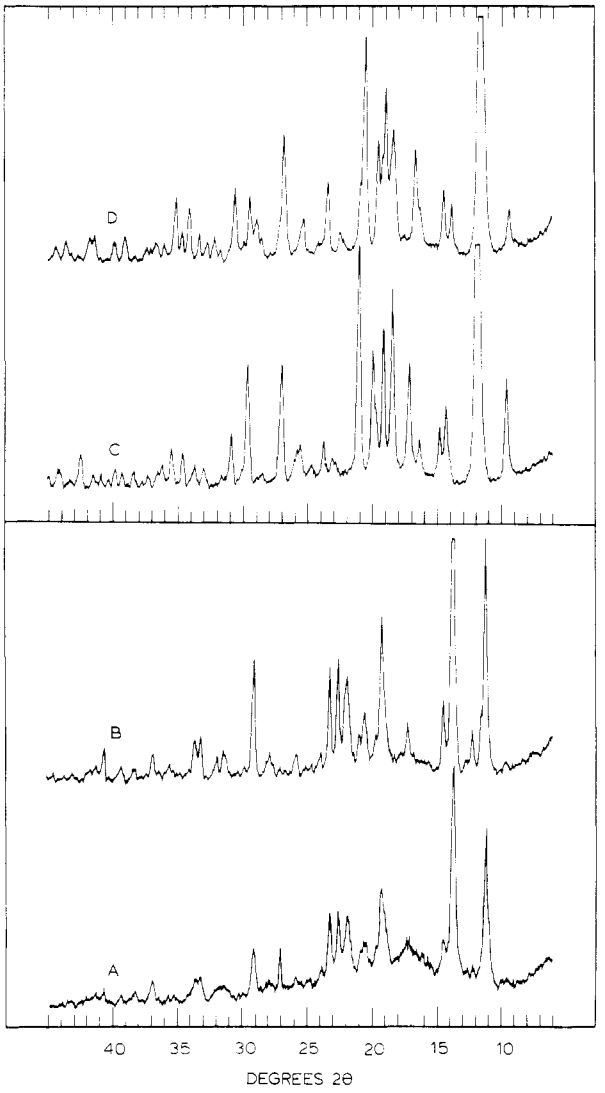


**Figure 4.** Room-temperature X-ray powder patterns for [Fe(Hthpu)(thpu)] (ground) (A), [Fe(Hthpu)(thpu)] (unperturbed) (B), [Fe(Hthpu)(thpu)]·$H_2O$ (C), and [Cr(Hthpu)(thpu)]·$H_2O$ (D).

nonhydrated ferric solid undergoes a thermally discontinuous spin-crossover transition. Before the details of this spin-crossover transition are discussed, the spectroscopic characteristics of the low-spin forms of both ferric materials are compared.

The hydrated complex is identified as being low spin by its room-temperature (299 K) magnetic moment of 2.48 $\mu_B$ ($\chi_M$(299 K) = 2.574 × $10^{-3}$ cgsu). Magnetic susceptibility studies also reveal that the nonhydrated ferric material is basically low spin below 220 K; a magnetic moment of 2.37 $\mu_B$ was found at 150 K.

In Figure 5 we illustrate the Q-band EPR spectra at 150 K of both low-spin materials. It is clear that the spectra for the hydrated and nonhydrated solids are quite different. The EPR signal of the hydrated ferric material is somewhat unusual for a low-spin ferric center of this type. That is, the rhombic signal exhibits relatively little **g**-tensor anisotropy ($g_1$ = 2.21, $g_2$ = 2.12, $g_3$ = 2.08) and, furthermore, all of the **g**-tensor components are substantially greater than the free-electron value of $g$ = 2.00. The most reasonable inference from these observations is that weak intermolecular magnetic exchange interactions effectively average the molecular **g** tensors on adjacent, crystallographically inequivalent metal centers. This explanation, which accounts for both the small **g**-tensor anisotropy and the low-field shifts of the **g**-tensor compoents, is supported by the observation of significant intermolecular interactions in the isostructural chromium lattice. In contrast, the $g$ values ($g_\parallel$ = 1.97, $g_\perp$ = 2.20) for the nonhydrated ferric solid are fairly typical for axially distorted low-spin

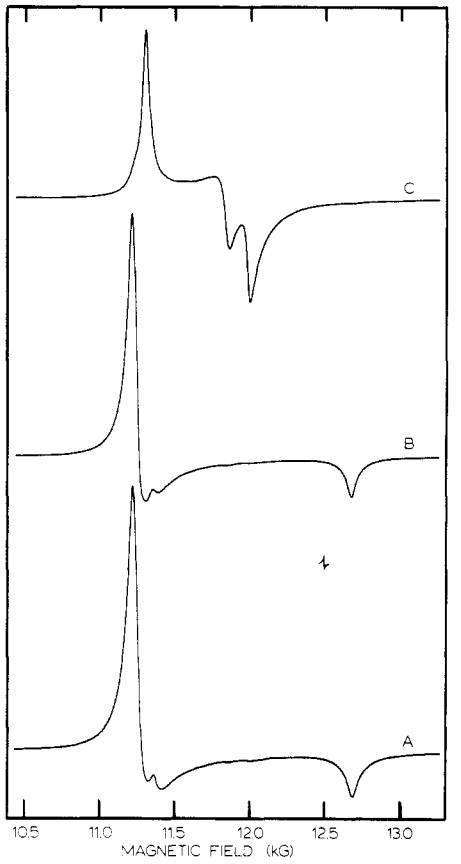


**Figure 5.** Q-Band EPR spectra at 150 K for [Fe(Hthpu)(thpu)] (ground) (A), [Fe(Hthpu)(thpu)] (unperturbed) (B), and [Fe(Hthpu)(thpu)]·$H_2O$ (C).

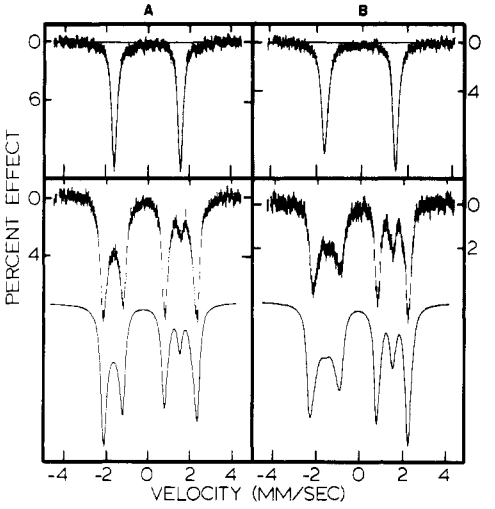


**Figure 6.** Column A: Mössbauer spectra for [Fe(Hthpu)(thpu)] at 152 K and 0 kG (upper) and at 10 K and 60 kG (lower). Column B: Mössbauer spectra for [Fe(Hthpu)(thpu)]·$H_2O$ at 140 K and 0 kG (upper) and at 80 K and 60 kG (lower). Simulations are shown as solid lines; the relevant parameters can be found in the text.

ferric centers. There is no clear evidence for intermolecular magnetic exchange effects. The $g$ values for the nonhydrated ferric material have been analyzed by following the method of Bohan.[40] It can be concluded that the unpaired electron is in an orbital of largely $d_{xy}$ character. The degeneracy of the $^2T_{2g}$ electronic state has been removed due to the combined effects of low-symmetry crystal field distortions and spin–orbit coupling; the first excited Kramers doublet of $^2T_{2g}$ origin is estimated to be 9000 $cm^{-1}$ higher

(40) Bohan, T. L. *J. Magn. Reson.* **1977**, *26*, 109.

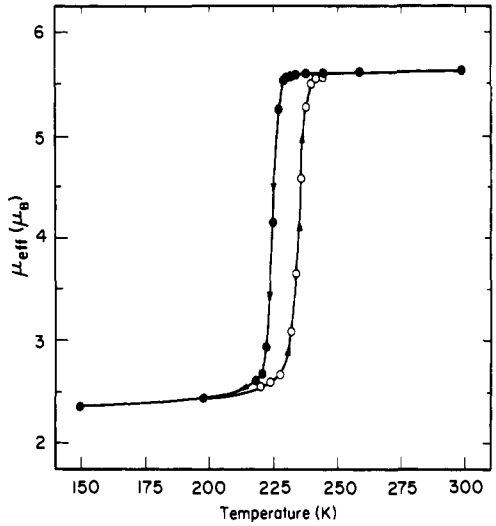


**Figure 7.** Effective magnetic moments of [Fe(Hthpu)(thpu)] as a function of temperature. Both cooling (●) and heating (○) curves are shown. The solid lines are drawn for purposes of clarity only and do not represent data fittings or simulations.

in energy than the ground-state Kramers doublet.

Mössbauer ($^{57}$Fe) spectra of [Fe(Hthpu)(thpu)] and [Fe(Hthpu)(thpu)]·$H_2O$ are illustrated in Figure 6. The zero-field Mössbauer parameters for the two forms are quite similar. For the nonhydrated material, the quadrupole splitting (QS) is 3.15 (1) mm/s and the center shift (CS) is 0.21 (1) mm/s. For the hydrated solid, QS = 3.12 (1) mm/s and CS = 0.18 (1) mm/s. All of these parameters are typical for low-spin ferric centers. The similarity of the parameters supports our assertion that the molecular structure of the [Fe(Hthpu)(thpu)] unit is identical in both solids. We also illustrate in Figure 6 the effect of applying a 60-kG magnetic field to the samples. The resulting "doublet–triplet" patterns were simulated as previously described.[30] Simulations were carried out with the assumption that the electron-spin relaxation rates are rapid relative to the $^{57}$Fe nuclear Larmor precession frequency. The hydrated compound was simulated with the following parameters: QS = −3.09 mm/s, $\eta = 0$, $g_\perp = 2.20$, $g_\parallel = 1.98$, $A_\perp = +25$ kG, $A_\parallel = -450$ kG. The parameters for the simulation of the nonhydrated material were found to be QS = −3.16 mm/s, $\eta = 0$, $g_\perp = 2.20$, $g_\parallel = 1.98$, $A_\perp = +25$ kG, and $A_\parallel = -150$ kG. Since QS is negative for both compounds, we can conclude that the unpaired electron occupies an orbital of essentially $d_{xy}$ character for both samples.

**The Spin-Crossover Transition for [Fe(Hthpu)(thpu)].** The discontinuous nature of the thermal spin-crossover transformation for [Fe(Hthpu)(thpu)] is evident from the variable-temperature magnetic susceptibility data illustrated in Figure 7. Thermal hysteresis is also apparent. That is, for the high-spin to low-spin transformation that occurs upon sample cooling, the transition temperature ($T_c(\downarrow)$) is 225 K. For the reverse transition, $T_c(\uparrow)$ is 235 K. The abruptness of the transition and the observation of thermal hysteresis lead us to conclude that the spin-state transformation involves a thermodynamic first-order phase transition.

The first-order nature of the spin-crossover transition is also revealed by variable-temperature EPR investigations. In Figure 8 is illustrated the temperature dependence of the low-spin EPR absorption intensity. These intensities, corrected for Curie law temperature dependence, are normalized relative to the low-spin intensity at 210 K. As with the magnetic susceptibility data, a thermal hysteresis of ~10 K is seen ($T_c(\downarrow) = 232$ K, $T_c(\uparrow) = 244$ K). The discrepancies in the transition temperatures determined by the magnetic susceptibility and resonance methods are due to the lower absolute temperature accuracy of the EPR experiment. It is interesting that, despite the Curie law corrections, the low-spin signal intensity continues to increase well below $T_c(\downarrow)$. A corresponding gradual decrease in the magnetic moment below $T_c(\downarrow)$ is also evident in Figure 7. It appears that there is a minor gradual

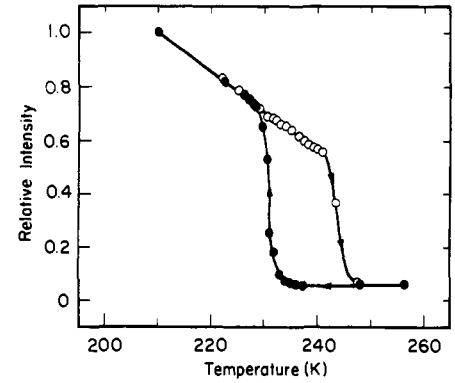


**Figure 8.** EPR intensities of the low-spin signal of [Fe(Hthpu)(thpu)] as a function of temperature. Data for cooling (●) and heating (○) cycles are shown. Solid lines are drawn for purposes of clarity only.

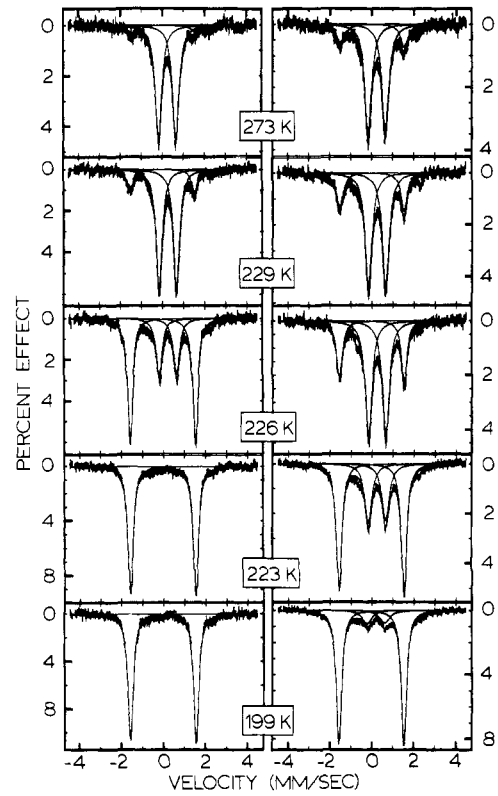


**Figure 9.** Left column: Mössbauer spectra for unperturbed [Fe(Hthpu)(thpu)] at selected temperatures. Right column: Spectra for [Fe(Hthpu)(thpu)] (ground) at selected temperatures.

spin-crossover transformation that accompanies the major discontinuous transition.

We were unable to analyze similarly the high-spin EPR intensity due to the unusual nature of the high-spin EPR signal for [Fe(Hthpu)(thpu)]. In fact, we were initially unable to even identify any signal as arising from the high-spin component. High-spin EPR signals for molecular solids of this type typically are found in the low-field region (1000–2500 G at X-band frequencies).[41] A careful inspection of the low-field region of the Q-band EPR spectrum of this sample at room temperature revealed a very broad signal (full width at half-height ~ 5 kG) centered near 8.5 kG ($g_{eff} \sim 3$). We attribute the extremely broad line width to short spin–spin relaxation times. Considering the short metal–metal distances noted for the hydrated chromium lattice, it is likely that similarly short iron–iron distances lead to enhanced dipole–dipole interactions and rapid spin–spin relaxation rates for [Fe(Hthpu)(thpu)].

(41) Wickman, H. H.; Klein, M. P.; Shirley, D. A. *J. Chem. Phys.* **1965**, *42*, 2115.

**Table V.** Mössbauer Parameters for [Fe(Hthpu)(thpu)] (Unperturbed), Two- and Four-Line Lorentzian Fits[a]

| T, K | $F$(HS)[b] | CS, mm/s | QS, mm/s | $\Gamma_{1/2}(-)$,[c] mm/s | $\Gamma_{1/2}(+)$,[d] mm/s | ln (area)[e] | $\chi^{2}$[f] |
|---|---|---|---|---|---|---|---|
| 273 | 0.92 (2) | 0.41 (1) | 0.82 (1) | 0.18 (1) | 0.18 (1) | 0.4756 | 0.58 |
| | | 0.23 (4) | 3.04 (8) | 0.21 (6) | 0.28 (9) | | |
| 250 | 0.91 (1) | 0.43 (1) | 0.82 (1) | 0.17 (1) | 0.18 (1) | 0.5944 | 0.67 |
| | | 0.19 (2) | 3.01 (3) | 0.17 (3) | 0.13 (2) | | |
| 239 | 0.89 (1) | 0.44 (1) | 0.83 (1) | 0.18 (1) | 0.18 (1) | 0.6944 | 0.60 |
| | | 0.19 (2) | 3.07 (3) | 0.17 (3) | 0.21 (3) | | |
| 234 | 0.89 (1) | 0.44 (1) | 0.83 (1) | 0.17 (1) | 0.18 (1) | 0.7105 | 0.72 |
| | | 0.20 (1) | 3.04 (3) | 0.17 (2) | 0.17 (2) | | |
| 231 | 0.90 (1) | 0.44 (1) | 0.82 (1) | 0.17 (1) | 0.17 (1) | 0.7030 | 1.02 |
| | | 0.18 (1) | 3.04 (2) | 0.16 (2) | 0.15 (2) | | |
| 229 | 0.85 (1) | 0.44 (1) | 0.82 (1) | 0.17 (1) | 0.17 (1) | 0.7522 | 0.94 |
| | | 0.18 (1) | 3.05 (2) | 0.17 (2) | 0.15 (1) | | |
| 226 | 0.35 (1) | 0.44 (1) | 0.82 (1) | 0.17 (1) | 0.18 (1) | 0.9018 | 0.70 |
| | | 0.18 (1) | 3.10 (1) | 0.15 (1) | 0.14 (1) | | |
| 223 | 0.0 | 0.18 (1) | 3.11 (1) | 0.15 (1) | 0.15 (1) | 0.9476 | 1.04 |
| 218 | 0.0 | 0.18 (1) | 3.12 (1) | 0.15 (1) | 0.15 (1) | 0.9636 | 0.79 |
| 199 | 0.0 | 0.19 (1) | 3.13 (1) | 0.15 (1) | 0.15 (1) | 1.0697 | 1.02 |
| 152 | 0.0 | 0.21 (1) | 3.15 (1) | 0.15 (1) | 0.15 (1) | 1.2550 | 0.69 |

[a] Parameters obtained by assuming equal areas for the two component peaks of a given quadrupole doublet. [b] High-spin fraction as estimated from relative absorption areas of high- and low-spin quadrupole doublets. [c] Half-width at half-height of the negative-velocity quadrupolar component. [d] Half-width at half-height of the positive-velocity quadrupolar component. [e] Natural logarithm of background-normalized area of total fitted spectrum. [f] $\chi^{2}$ value indicating quality of data and of fit to 11 adjustable parameters for a four-line spectrum or 6 adjustable parameters for a two-line spectrum.

**Table VI.** Mössbauer Parameters for [Fe(Hthpu)(thpu)] (Ground), Four-Line Lorentzian Fits[a]

| T, K | $F$(HS)[b] | CS, mm/s | QS, mm/s | $\Gamma_{1/2}(-)$,[c] mm/s | $\Gamma_{1/2}(+)$,[d] mm/s | ln (area)[e] | $\chi^{2}$[f] |
|---|---|---|---|---|---|---|---|
| 273 | 0.81 (1) | 0.40 (1) | 0.82 (1) | 0.19 (1) | 0.29 (1) | 0.4167 | 0.71 |
| | | 0.18 (1) | 3.05 (3) | 0.27 (3) | 0.22 (2) | | |
| 250 | 0.80 (1) | 0.43 (1) | 0.82 (1) | 0.19 (1) | 0.19 (1) | 0.5764 | 0.86 |
| | | 0.19 (1) | 3.07 (2) | 0.24 (2) | 0.23 (2) | | |
| 239 | 0.80 (1) | 0.43 (1) | 0.83 (1) | 0.18 (1) | 0.18 (1) | 0.6381 | 0.74 |
| | | 0.18 (1) | 3.07 (1) | 0.19 (1) | 0.20 (1) | | |
| 234 | 0.78 (1) | 0.43 (1) | 0.83 (1) | 0.19 (1) | 0.19 (1) | 0.6814 | 0.99 |
| | | 0.17 (1) | 3.07 (1) | 0.20 (1) | 0.19 (1) | | |
| 231 | 0.78 (1) | 0.43 (1) | 0.82 (1) | 0.19 (1) | 0.19 (1) | 0.6768 | 1.09 |
| | | 0.19 (1) | 3.06 (1) | 0.19 (1) | 0.17 (1) | | |
| 229 | 0.76 (1) | 0.43 (1) | 0.82 (1) | 0.19 (1) | 0.19 (1) | 0.7012 | 1.03 |
| | | 0.19 (1) | 3.05 (1) | 0.20 (1) | 0.18 (1) | | |
| 226 | 0.70 (1) | 0.43 (1) | 0.82 (1) | 0.19 (1) | 0.19 (1) | 0.7435 | 0.98 |
| | | 0.19 (1) | 3.08 (1) | 0.17 (1) | 0.16 (1) | | |
| 223 | 0.38 (1) | 0.43 (1) | 0.83 (1) | 0.20 (1) | 0.21 (1) | 0.8388 | 1.27 |
| | | 0.18 (1) | 3.09 (1) | 0.16 (1) | 0.15 (1) | | |
| 218 | 0.25 (1) | 0.41 (1) | 0.86 (1) | 0.25 (1) | 0.26 (1) | 0.8947 | 0.86 |
| | | 0.18 (1) | 3.09 (1) | 0.16 (1) | 0.15 (1) | | |
| 199 | 0.15 (1) | 0.39 (1) | 0.85 (2) | 0.27 (2) | 0.28 (2) | 1.003 | 1.40 |
| | | 0.19 (1) | 3.09 (1) | 0.16 (1) | 0.15 (1) | | |

[a] Parameters obtained by assuming equal areas for the two component peaks of a given quadrupole doublet. [b] High-spin fraction as estimated from relative absorption areas of high- and low-spin quadrupole doublets. [c] Half-width at half-height of the negative-velocity quadrupolar component. [d] Half-width at half-height of the positive-velocity quadrupolar component. [e] Natural logarithm of background-normalized area of total fitted spectrum. [f] $\chi^{2}$ value indicating quality of data and of fit to 11 adjustable parameters.

Variable-temperature $^{57}$Fe Mössbauer spectra, illustrated in Figure 9 and listed in Table V, are consistent with the discontinuous nature of the spin-crossover transition. At 272 K, the inner high-spin quadrupole doublet accounts for over 90% of the total absorption area. As the sample temperature is decreased, the intensity of the high-spin doublet decreases dramatically between 229 and 226 K and goes to zero below 223 K. The intensity of the outer low-spin quadrupole-split doublet increases in the same temperature region.

It is interesting that the high-spin ferric quadrupole-split doublet exhibits such small line half-widths ($\Gamma_{1/2} \sim 0.2$ mm/s). High-spin ferric centers, if they are well isolated in molecular solids, can exhibit line half-widths greater than 1 mm/s.[42] Such line broadening is the result of long paramagnetic relaxation times. The narrow lines for high-spin [Fe(Hthpu)(thpu)] certainly indicate that the electron-spin relaxation rates are more rapid than the $^{57}$Fe nuclear Larmor precession frequency, and no magnetic broadening is observed. As before (vide supra), we attribute the short relaxation times to spin–spin mechanisms enhanced by short dipole–dipole (i.e., Fe–Fe) distances. Wignall[42] has examined several high-spin ferric systems and noted that, for Fe–Fe distances of 6–7 Å, short paramagnetic relaxation times and narrow Mössbauer line widths were observed. Longer distances (>7 Å) led to broad line widths and incipient magnetic patterns. Although we have no *direct* knowledge of the Fe–Fe distances in [Fe(Hthpu)(thpu)], the short Cr–Cr distances (<7 Å; vide supra) in the [Cr(Hthpu)(thpu)]·$H_2O$ lattice indicate that the Fe–Fe distances are probably quite short.

The effect of sample perturbations on discontinuous spin-crossover transitions has been well documented.[10-12,43,44] The effect of grinding a microcrystalline sample of [Fe(Hthpu)(thpu)] is illustrated in Figures 9 and 10. It is evident from both figures that sample grinding leads to a more gradual and less complete spin-crossover transformation. The Mössbauer spectra (Figure 9 and Table VI) reveal the same low- and high-spin species that were seen for the unperturbed, microcrystalline sample. That is,

(42) Wignall, J. W. G. *J. Chem. Phys.* **1966**, *44*, 2462.

(43) König, E.; Ritter, G.; Kulshreshtha, S. K. *Inorg. Chem.* **1984**, *23*, 1144.
(44) König, E.; Ritter, G.; Kulshreshtha, S. K.; Csatary, N. *Inorg. Chem.* **1984**, *23*, 1903.

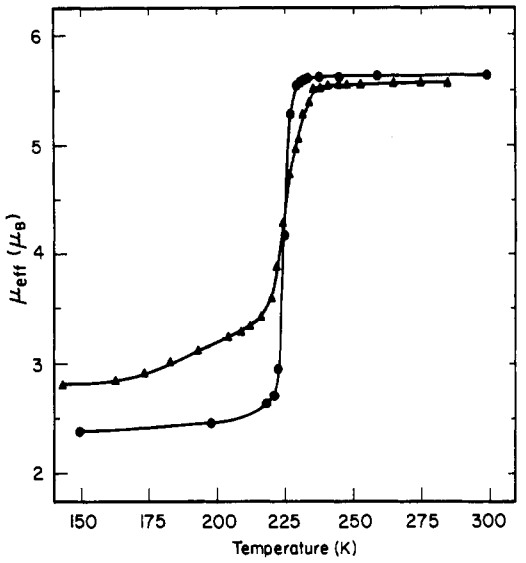


**Figure 10.** Effective magnetic moments of unperturbed [Fe(Hthpu)(thpu)] (●) and ground [Fe(Hthpu)(thpu)] (▲) as a function of temperature. Solid lines are drawn for purposes of clarity only.

the temperature dependences of the intensities of the high- and low-spin absorptions change upon sample grinding, but no new absorptions are seen. X-ray powder diffraction and EPR experiments (Figures 4 and 5, respectively) also show no evidence for sample decomposition upon grinding. Haddad et al.[10-12] have interpreted similar observations in terms of the nucleation and growth mechanism of phase transitions. According to this mechanism, at the transition temperature where the free energy of the incipient phase becomes lower, the phase transition occurs by a series of steps: (1) individual molecules of the incipient phase must nucleate into the "old" phase; (2) the nuclei then combine to form domains of sufficient size so that domain growth can occur; and (3) the domains grow, and the new phase exists. The introduction of defects by grinding appears to decrease the activation energy of nucleation and to increase the activation energy of domain growth. Consequently, the spin-crossover transition is smeared-out; the high- and low-spin molecules can exist far from the transition temperature, presumably at surface or lattice defect sites.

## Comments and Conclusions

A number of theoretical attempts have been made to predict the thermodynamics of the bulk solid-state spin-crossover transformation.[45,46] In order to predict thermally *discontinuous* spin-crossover transformations, it has generally been necessary to invoke the use of some intermolecular interaction parameter. That is, the fundamental difference between a continuous (equilibrium-like) spin-crossover transformation and a first-order spin-crossover phase transition is that there is a cooperative aspect to the latter type. *Inter*molecular interactions are important. Purcell and Edwards,[47] by using the phenomenological model of Slichter and Drickamer,[48] have demonstrated that the cooperative nature of a given spin-crossover transformation depends not only upon the energy of these intermolecular interactions but also upon the temperature of the spin-state transition.

Despite the successes (and failures) of these theories, it is still largely an experimental task to uncover the *microscopic* origins of the intermolecular interactions responsible for discontinuous spin-crossover transitions. Earlier in this report, we noted that, as a class, the ferric thiosemicarbazone complexes are unique among *ferric* spin-crossover solids in that they show a relative abundance of *discontinuous* spin-crossover transitions. The ferric thiosemicarbazones are also unique among ferric spin-crossover solids in that they possess an abundance of potential sites for intermolecular hydrogen-bonding interactions. As we have demonstrated for [Cr(Hthpu)(thpu)]·$H_2O$ and as has been seen for other metal thiosemicarbazones,[38,39] intermolecular hydrogen-bonding interactions are indeed significant and result in a relatively strong coupling of the monomeric units in the solid state. It is quite likely, then, that for [Fe(Hthpu)(thpu)] the cooperative aspect of the spin-crossover transformation is due to the extended coupling of ferric complexes through intermolecular hydrogen bonds.

Although we suggest that intermolecular hydrogen-bonding interactions may lead to cooperativity and discontinuities in the spin-crossover transitions for ferric thiosemicarbazones, we certainly cannot attribute *all* discontinuous transitions to this single origin. The details of intermolecular interactions undoubtedly depend upon subtle crystal-packing and lattice properties. These will be, to some extent, unique for each solid. It is interesting, however, that hydrogen-bonding interactions have been noted[49,50] for other structurally characterized spin-crossover solids that undergo discontinuous thermal spin-state transitions.

**Acknowledgment.** We are grateful for support from National Institutes of Health Grant HL13652.

**Registry No.** $H_2$thpu, 10418-09-4; [Fe(Hthpu)(thpu)], 97921-09-0; [Cr(Hthpu)(thpu)]·$H_2O$, 97995-60-3; pyruvic acid, 127-17-3; thiosemicarbazide hydrochloride, 4346-94-5.

**Supplementary Material Available:** Listings of structure factors and thermal parameters for [Cr(Hthpu)(thpu)]·$H_2O$ and tables of magnetic susceptibility and EPR data (12 pages). Ordering information is given on any current masthead page.

(45) Gütlich, P. *Struct. Bonding (Berlin)* **1981**, *44*, 176.
(46) Zimmermann, R. *J. Phys. Chem. Solids* **1983**, *44*, 151.
(47) Purcell, K. F.; Edwards, M. P. *Inorg. Chem.* **1984**, *23*, 2620.
(48) Slichter, C. P.; Drickamer, H. G. *J. Chem. Phys.* **1972**, *56*, 2142.
(49) Katz, B. A.; Strouse, C. E. *J. Am. Chem. Soc.* **1979**, *101*, 6214.
(50) Mikami, M.; Konno, M.; Saito, Y. *Chem. Phys. Lett.* **1979**, *63*, 566.